

Self-maintaining CD103⁺ cancer-specific T cells are highly energetic with rapid cytotoxic and effector responses

Megat Abd Hamid^{1,2}, Huw Colin-York², Nasullah Khalid Alham^{3,4}, Molly Browne⁵, Lucia Cerundolo⁵, Ji-Li Chen², Xuan Yao^{1,2}, Samara Rosendo-Machado², Craig Waugh⁶, David Maldonado-Perez⁵, Emma Bowes⁵, Clare Verrill^{4,5}, Vincenzo Cerundolo^{1,2}, Christopher P. Conlon¹, Marco Fritzsche^{2,7}, Yanchun Peng^{1,2,8}, Tao Dong^{1,2,8}*

¹Chinese Academy of Medical Sciences (CAMS)-Oxford International Centre for Translational Immunology, CAMS Oxford Institute, Nuffield Department of Medicine, University of Oxford, OX3 7FZ, Oxford, UK. ²Medical Research Council (MRC) Human Immunology Unit, MRC Weatherall Institute of Molecular Medicine, Radcliffe Department of Medicine, University of Oxford, OX3 9DS, Oxford, UK. ³Institute of Biomedical Engineering, Department of Engineering Science, University of Oxford, OX3 7DQ, Oxford, UK. ⁴Oxford National Institute of Health Research (NIHR) Biomedical Research Centre, University of Oxford, John Radcliffe Hospital, OX3 9DU, Oxford, UK. ⁵Nuffield Department of Surgical Sciences, University of Oxford, Oxford, John Radcliffe Hospital, OX3 9DU, Oxford, UK. ⁶Flow Cytometry Facility, Weatherall Institute of Molecular Medicine, University of Oxford, OX3 9DS, Oxford, UK. ⁷Kennedy Institute of Rheumatology, University of Oxford, OX3 7FY, Oxford, UK. ⁸ contributed equally to this work

***Correspondence(s):** Tao Dong; mailing address: Nuffield Department of Medicine, University of Oxford, OX3 7FZ, Oxford, UK; email address: tao.dong@imm.ox.ac.uk; telephone number: +441865222443; fax: +441865222502.

Running title: Effective killing by highly energetic TGFβ⁺CD103⁺ CTLs

Keywords: CD103; antigen sensitivity; rapid killing; high energy potential; T cell death

Conflict of interest statement: The authors declare no potential conflicts of interest.

Funding: This work was supported by the Chinese Academy of Medical Sciences (CAMS) Innovation Fund for Medical Sciences (CIFMS), China (grant number: 2018-I2M-2-002); Medical Research Council (MRC), United Kingdom (MR/L018942/1 and MRC Human Immunology Unit Core); John Fell Fund (R45603/CN002). M. Abd Hamid is funded by the Malaysia's King Scholarship, MF and HC-Y are funded by Wellcome Trust (212343/Z/18/Z) and EPSRC (EP/S004459/1), CV and NK-A research time is supported, as well as DMP is funded by the National Institute of Health Research (NIHR) Oxford Biomedical Research Centre (BRC) (Molecular Diagnostics Theme/Multimodal Pathology Subtheme). We declare no conflicts of interest.

Abstract

Enrichment of CD103⁺ tumor-infiltrating T lymphocytes (TILs) is associated with improved outcomes in patients. However, the characteristics of human CD103⁺ cytotoxic CD8⁺ T cells (CTLs) and their role in tumor control remains unclear. We investigated the features and antitumor mechanisms of CD103⁺ CTLs by assessing T-cell receptor (TCR)–matched CD103⁺ and CD103[−] cancer-specific CTL immunity *in vitro* and its immunophenotype *ex vivo*. Interestingly, we found that differentiated CD103⁺ cancer-specific CTLs expressed the active form of TGFβ1 to continually self-regulate CD103 expression, without relying on external TGFβ1-producing cells. The presence of CD103 on CTLs improved TCR antigen sensitivity which enabled faster cancer recognition and rapid antitumor cytotoxicity. These CD103⁺ CTLs had elevated energetic potential and faster migration capacity. However, they had increased inhibitory receptor co-expression and elevated T-cell apoptosis following prolonged cancer exposure. Our data provide fundamental insights into the properties of matured human CD103⁺ cancer-specific CTLs, which could have important implications for future designs of tissue-localized cancer immunotherapy strategies.

Introduction

CD103 (integrin α_E) is primarily expressed on tissue-resident memory T cells (Trm) and is widely recognized as a key player in viral tissue-localized immunity, including in the clearing of murine herpes simplex virus (HSV) skin infection and murine lung influenza infection (1,2). Increasing interest is seen for CD103's potential in human cancer control and eradication. It has been shown that enrichment of CD103⁺ tumor-infiltrating T lymphocytes (TILs) is associated with improved outcomes in cancer patients either with melanoma, colorectal, urothelial, or early stage lung cancers (3-7).

The induction and development of CD103 expression on developing T cells require initial antigenic contact and the presence of microenvironmental TGFβ1 cues, presumably produced by murine Batf3-dependent dendritic cells (DCs), human CD1c⁺ conventional DCs, and regulatory T cells (Tregs) (8-10). Impaired CD103⁺ Trm populations in tissues occurs in the absence of TGFβ1, as well as the inactivation of its

receptor on T cells (11). However, because DCs in the tumor microenvironment are known to be dysfunctional (12-14), it remains unclear how continuous CD103 expression on differentiated cancer-specific CTLs is maintained, especially during prolonged cancer exposure.

Human cancer testis antigens (CTAs), such as synovial sarcoma X-2 (SSX-2) and New York-esophageal squamous cell carcinoma-1 (NY-ESO-1) proteins, are a class of antigens that are not expressed in healthy tissue but are upregulated in cancer cells. Although CTA-specific CTLs are promising targets for immunotherapy, they have low-affinity TCRs and sensitivity to tumor antigen/MHC complexes (15,16). This can result in an overall impaired efficacy of antitumor T-cell responses and thus, poor tumor control. Interestingly, CD103 molecules accumulate in the immunological synapse following T-cell interaction with autologous cancer cells (17,18). It is, therefore, possible that CD103 could play a role in TCR-mediated antitumor CTL immune responses.

Tumor-reactive TILs with CD103 and CD39 co-expression are shown to have increased inhibitory receptor expression (19). However, because enrichment of CD103⁺ TILs is known to improve clinical outcomes in patients, its possible dysfunctional immunophenotype raises uncertainty about its relevance as a primary target for immunotherapy and its significance to overall antitumor immune activities. Therefore, a comprehensive understanding of the properties of human CD103⁺ CTLs and the potential contribution of CD103 towards antitumor T-cell effector and cytotoxic responses is urgently required.

In this study, we sought to investigate CD103-mediated characteristics and immune mechanisms of human cancer-specific CTLs. We found that differentiated cancer-specific CTLs could self-produce an activated form of TGFβ1 to maintain continual CD103 expression, without reliance on external TGFβ1 cues from other cells. These CD103⁺ cancer-specific CTLs had increased tumor antigen sensitivity and elevated metabolic potential. Using live cell imaging, we clearly demonstrated that CD103⁺ CTLs had faster cancer recognition, which led to rapid and cumulative E-Cadherin⁺ cancer cell killing following prolonged cancer exposure. We also demonstrated that CD103^{high}CD39⁺ TILs, but not CD103^{low}CD39⁺ TILs, had cumulative

inhibitory receptor co-expression *ex vivo* and elevated caspase 3–mediated apoptosis after prolonged exposure to cancer. Taken together, our study highlights key antitumor features of CD103⁺ cancer-specific CTLs and provides information that will help in the design of better and more effective tissue-localized T cell–based cancer immunotherapies.

Materials and Methods

Study design and patients

This study was approved by the Oxford Radcliffe Biobank (ORB) research ethics committee (reference number: 09/H0606/5+5), based on the guidelines of the Declaration of Helsinki. Tumor and paratumor tissues were collected from five lung cancer patients for *ex vivo* analysis. Criteria chosen of these patients include non-metastatic, early TNM stage, carcinoma-confirmed cancer patients. Sizes of tissue samples collected are kept consistent between each patient, (resection volume of no less than 0.5x0.5x0.5 cm), and the patients did not have metastatic disease. Samples were collected during patients' surgery, stored in Roswell Park Memorial Institute 1640 (RPMI 1640) medium on ice, and immediately processed. The tumor samples were confirmed as malignant using immunohistopathology. Written informed consent was obtained from all subjects prior to the inclusion in the study. Paired tumor and paratumor tissue samples from five lung cancer patients were used for *ex vivo* data analysis, as described below. Peripheral blood was obtained from patients with confirmed presence of cancer-specific T cells for the *in vitro* functional assays. The patients' clinical details are described as in **Supplementary Table S1**.

Generating CD103⁺ and CD103[−] cancer-specific CTLs

All *in vitro* functional experiments were conducted using clonally expanded cancer-specific CTLs that were generated from cancer patients, using a well-established human antigen-specific T cells generation technique as previously described (20-22). A detailed flow chart of the generation of human cancer-specific CTLs is shown in

Supplementary Fig. S1. Briefly, mononuclear cells (consisting of a mixture of T cells, B cells, and antigen-presenting cells) from individual patients' blood were isolated using a Ficoll-Hypaque density gradient centrifugation. Around 3 million cells were then stimulated with either cancer SSX2₄₁₋₄₉-specific KV9 peptide (KASEKIFYV) or NY-ESO-1₁₅₇₋₁₆₅-specific SC9 peptide (SLLMWITQC) (10 µg/mL; Peprotech, UK) in RPMI-1640 supplemented with 10% v/v heat-inactivated human AB serum (National Blood Service, UK), 2mM L-Glutamine, 1% v/v (500 U/mL) penicillin/streptomycin (Sigma-Aldrich, UK), and recombinant human IL2 (200 U/mL) (Peprotech, UK) (H10) at 37°C for 14 days. B cells and antigen-presenting cells within the isolated mononuclear cell mixture present the peptides to the T cells for activation and proliferation.

After 14 days, CD103⁺ and CD103⁻ cancer-specific CTLs were sorted using a PE-conjugated HLA class I tumor peptide tetramer [HLA-A2 KV9 or HLA-A2 SC9 tetramers; in-house preparation as in (22,23)], FITC-CD8 (clone: SK1; BD Biosciences; RRID:AB_2739852), and BV711-CD103 (Ber-ACT8, Biolegend; RRID: AB_2629650) using a BD Aria IIIu (BD Biosciences). The purity of the sorted population was confirmed at 95% purity. The isolated cells were then clonally expanded and cultured *in vitro*. The sorted cells were cultured with 2 million irradiated cone blood cells (Oxford NHS Blood and Transplant Service) for 14 days in H10 medium (as described above), supplemented with recombinant human IL2 (200 U/mL; Peprotech, UK). The T-cells were confirmed for antigen-specificity using HLA-A2 KV9 and SC9 tetramers staining, ran on Attune NXT flow cytometry (ThermoFisher, UK), analyzed using FlowJo v.10 (TreeStar Inc.). The validated T cells were then stored in several batches for future assays and used for all *in vitro* functional assays. T-cell cultures were tested for mycoplasma monthly, maintained for 2 months for every assay, passaged once after every thaw, and re-authenticated again using the tetramers method after every thawing and passage

Target cell lines used for *in vitro* functional assays

All the following *in vitro* functional assays were performed by culturing CTLs with target cells [HCT116 (CCL-247; obtained from ATCC, VA, US, in 2017) or THP-1 (TIB-202;

from ATCC, VA, US, in 2017)]. Each commercial cell line was authenticated every six months, with specific surface markers known to be expressed by each cell line, ran on Attune Nxt flow cytometer (ThermoFisher), and analyzed on FlowJo v.10 (TreeStar Inc.). Antibodies used include APC–E-Cadherin (67A4, Biolegend; RRID: AB_756069) for HCT116 or APC-CD33 (WM53; Biolegend; RRID: AB_314352) for THP-1. Each cell line was cultured *in vitro* as per the manufacturer's guidelines. Briefly, HCT116 cells were cultured at 2 million cells in McCoy 5'A medium (ThermoFisher), whereas THP-1 was cultured in RPMI 1640 supplemented with 10% v/v fetal calf serum (ThermoFisher) for 4 days prior to any T-cell functional assays. Each cell line was tested for mycoplasma upon receipt from the vendor and every month.

Prior to culturing, target cells were externally loaded with corresponding peptides (SSX-2 or NY-ESO-1, 10 µg/mL) at 37°C for 1 hour to enable the loading and presentation of the peptides on the MHC complex on the target cell surface. HCT116 is a commercially available cancer cell line that is known to be HLA-A2⁺, E-Cadherin⁺ (the ligand for CD103) and does not express SSX-2 and NY-ESO-1 proteins (24-27). Another condition was also included by using THP-1 as target cells, which is E-Cadherin⁻ HLA-A2⁺ SSX-2⁻ NY-ESO-1⁻.

Cytokine production assessment

To assess cytokine production, 0.2 million CTLs were either treated with blocking anti-CD103 (15 µg/mL; Ber-ACT-8, Biolegend) or isotype control (mouse IgG1k; 15 µg/mL; Biolegend) for 20 minutes. 50 µL of supernatants were collected and diluted at ratio 1:5 in RPMI, after 48 hours of coculturing T cells with peptide-loaded HCT116 target cells at an E:T ratio of 1:10 at 37°C. IFN γ was quantified using the Bio-Plex ProTM Human Cytokine Assay (BioRad) and ran on Bio-Plex 200 and analyzed using Bio-Plex Manager (Bio-Rad). Concentration was calculated automatically by the Bio-Plex Manager. Briefly, fluorescence intensity was measured by the machine and concentration was quantified based on standard (diluted by 1:100) for 5 times, with known original concentration. Standard was provided by the vendor (Bio-Rad) and purchased before every Bio-Plex assay. Cytokine concentration was then corrected

using control (supernatant without T-cells present). TGF β 1 presence in the supernatant was evaluated using the Human TGF-beta-1 Quantikine ELISA kit (R&D Systems), according to manufacturer's instructions. Briefly, 50 μ L of supernatant was used every time, diluted 1:20 in RPMI 1640, ran on MultiSkan FC Microplate Photometer (ThermoFisher). The same control and concentration correction method was used for the ELISA as per used for the Bio-Plex assay.

Intracellular cytokine staining

0.2 million CTLs were treated with monensin (10 μ g/mL) and brefeldin A (19 μ g/mL; provided by BD Biosciences) for 15 minutes prior to coculturing with peptide-loaded HCT116 target cells at an E:T ratio of 1:10 at 37°C for 5 hours. Cells were then fixed with Cytofix/CytopermTM (BD Biosciences) and stained with conjugated antibodies including Alexa Fluor488-IFN γ (B27; BD Biosciences; RRID: AB_396827), PE-LAP (TW4-6H10; Biolegend; RRID: AB_10639862), and APC-CD107a (H4A3; BD Biosciences; RRID: AB_1727417). Samples were ran on Attune Nxt flow cytometer (ThermoFisher), and analyzed on FlowJo V.10 (TreeStar Inc.). Evaluation of responses following anti-CD103 treatment was carried out using the antibody blocking treatment mentioned above.

CFSE-based CTL killing assay

HCT116 target cells were initially stained with 0.5 μ M CFSE (ThermoFisher, UK) before peptide-loading at four different concentrations for 1 hour (2 μ g/mL, 1 μ g/mL, 0.4 μ g/mL, 0.08 μ g/mL), and cocultured with CTLs at E:T ratio of 1:10 at 37°C for 6 hours. For the prolonged cancer exposure assay, target cells were cocultured with CTLs hourly for up to 12 hours. Cells were then stained with 7-AAD (BD Biosciences) and either APC-E-Cadherin (67A4, Biolegend; RRID: AB_756069) for HCT116 or APC-CD33 (WM53; Biolegend; RRID: AB_314352) for THP-1. Assessment of cell death was based on the CFSE⁺7-AAD⁻ population present. Apoptosis-induced death was measured hourly by the presence of activated caspases in CTLs following 12 hours' exposure to target cells,

using the FITC-active caspase-3 apoptosis kit (BD Biosciences), ran on Attne Nxt flow cytometer (ThermoFisher) and analyzed on FlowJo v.10 (TreeStar Inc.).

TCR sequencing

Briefly, the T-cell receptor was sequenced by isolating mRNA from CTLs using the RNAeasy Mini Kit (Qiagen, Germany) and cDNA was synthesized from 500 ng mRNA using the SMARTer RACE cDNA Amplification kit (Takara), as per manufacturer's instruction. Briefly, cDNA was PCR-amplified for CDR3 region of both alpha and beta TCR chains using the PCR Advantage Kit (Takara) using the following primers for TRAC: 5'- GGAACCTTTCTGGGCTGGGGAAGAAGGTGTCTTCTGG-3' and for TRBC: 5'- TGCTTCTGATGGCTCAAACACAGCGACCT-3' and run on a 1% agarose gel for PCR band confirmation (TRAV band at 700bp and TRBV band at 500bp). PCR product was then purified using NucleoSpin Gel and PCR clean-up kit (Macherey-Nagel, Germany) and transformed into TOP10 competent cells (ThermoFisher, UK) before being plated on LB agar media at 50 µL per plate, as per manufacturer's instructions. Colony PCR was performed using 200 ng of initial PCR product to amplify the product before isolating the plasmid DNA using the Spin Miniprep kit (Qiagen, Germany). The purified plasmid DNA was then sent for sequencing at a 100 nM concentration, performed by Timothy Rostron and John Frankland of the Sequencing Facility, Weatherall Institute of Molecular Medicine, University of Oxford. Sequencing data of T-cell clones are described in the Results section and Supplementary Table S2.

Migration transwell assay

Three days before coculture of cancer-specific CTLs with 2 µg/mL peptide-loaded HCT116 cells, or THP-1 cells were seeded in a 24-well plate at 0.25 million cells/mL in DMEM, supplemented with 10% v/v fetal calf serum (Sigma-Aldrich, UK), 2mM L-glutamine, and 1% v/v (500 U/mL) penicillin/streptomycin (Sigma-Aldrich, UK). Target cells were incubated at 37°C for two hours, to allow cancer cell lines to form a monolayer and produce cytokines and chemokines. 1 million cells/mL CTLs were seeded on a 5 µm pore size transwell insert (Corning) and rested in 37°C incubator to

let the cells to settle to the bottom of the insert. After 1 hour, inserts were transferred to the 24-well plates containing the target cells and further incubated at 37°C for 2 hours. Following this, cells in each well were harvested, stained with LIVE/DEAD® Fixable Aqua Dead Cell Stain Kit (ThermoFisher, UK) at 4°C for 20 minutes, with subsequent PerCP/Cy5.5-CD8 (SK1; BD Biosciences; RRID:AB_2687497) staining at the same temperature and duration before quantified using Attune Nxt flow cytometer (ThermoFisher), and analyzed using FlowJo v.10 (TreeStar Inc.). Migration was calculated as the total number of live CTLs present in the 24-well plate. Evaluation of migration following anti-CD103 treatment was performed by initially treating CTLs with 15 µg/mL anti-CD103 or isotype control for 20 minutes before coculture. Imaging was performed using IncuCyte (Essence Bioscience) and quantified using ImageJ (NIH).

Mitochondrial and glycolytic analysis

CTLs were starved of IL2 three days prior to the experiment. After which, 7.5 million cells/mL CTLs were seeded on a Seahorse 96-well microplate (Seahorse Biosciences) containing XF complete media (for mitochondrial stress: DMEM plus 2 mM L-glutamine, 10 mM glucose, and 1 mM sodium pyruvate; for glycolytic stress: DMEM plus 2 mM L-glutamine). For the mitochondrial stress assay, assay was performed using Seahorse XF cell mito stress test kit, per manufacturer's instruction. Briefly, cells were injected initially with 1 mM oligomycin (inhibits ATP synthase complex V), then 1.5 mM carbonyl cyanide-4 (trifluoromethoxy) phenylhydrazone (FCCP; disrupts mitochondrial membrane potential), and finally with 100 µM rotenone (complex I inhibitor)/1 mM antimycin A (complex III inhibitor) at 20-minute intervals. For the glycolysis stress assay, assay was performed using Seahorse XF glycolysis stress test kit, per manufacturer's instruction. Briefly, cells were injected initially with 10 mM glucose, then 1 µM oligomycin, and finally with 50 mM 2-deoxy-glucose (2-DG; inhibitor of glycolysis) at 20 minutes intervals. Drug injection and analysis were performed by the Seahorse XF96 extracellular Flux analyzer (Seahorse Biosciences), with Seahorse Wave software (Agilent). The oxygen consumption rate (OCR) was recorded as pmol/min, whereas the extracellular acidification rate (ECAR) was recorded as mpH/min.

Live cell imaging

HCT116 or THP-1 cells were seeded at 0.05 million cells/ml per well in μ -slide 8-well glass bottom (Ibidi; cat number: 80841) in DMEM supplemented with 10% v/v fetal calf serum, 2 mM L-glutamine, and 1% v/v (500 U/mL) penicillin/streptomycin and incubated at 37°C for 2 days to allow cells to attach to the glass, grow, and produce cytokines and chemokines. Peptide (1 μ g/mL) was then added 1 hour before imaging, with the seeded target cell culture supplemented with 2 mM calcium chloride and Alexa-Fluor 647-Annexin V (5 μ L/well; Cat. number: A23204; ThermoFisher, UK). The imaging chamber was then loaded onto a spinning disk confocal microscope (Zeiss Cell Observer Spinning Disc Confocal; Zeiss, Germany), equipped with a 10X air objective, enclosed in an incubator chamber at 37°C and 5% CO₂. CTLs were then added at 2 million cells/mL and imaging was carried out on each individual well in parallel, using brightfield and 632 nm excitation at 20% of maximum. Imaging was carried out for 12 hours at 1 frame per four minutes. Annexin V–positive staining is illustrated in the figures as blue.

For the killing duration assay, target cells and CTLs were prepared as described above. CTLs were then labelled with calcium sensitive probe Fluo4-AM (10 μ g/mL; F14201, Sigma Aldrich, UK) and 2.5 μ M probenecid (Sigma Aldrich, UK) and incubated at 37°C for 5 minutes. CTLs were then washed twice in fresh medium containing probenecid. The imaging chamber was set up as described above. Fluo4-AM–labelled CTLs were added to each well of the imaging slide before imaging was carried out using brightfield and 488 nm excitation at 20% of maximum. Imaging was carried out for 2 hours at 4 frames per minute. Fluo4-AM–positive staining is illustrated in the figures as red. All images were analyzed using ImageJ (NIH, US).

Flow cytometry staining

Freshly collected tissues were cut into 1 mm³ pieces and digested with the human tumor dissociation kit in C-tubes (Miltenyi Biotec) following the protocol provided by the

manufacturer. The C-tube was fixed on a rotator (Miltenyi Biotec) and rotated at low speed while the tumor tissue was enzymatically digested at 37 °C. GentleMACS Octodissociator (Miltenyi Biotec) was used to physically disrupt the tissue between incubation with enzymes. At the end of dissociation, the cells were filter through 100 µM strainer to obtain the single-cell suspension. The single cells were pelleted and washed once with 50 mL RPMI (Thermo Scientific Heraeus, 40R) at 300 x g for 10 minutes at room temperature. The cells were resuspended in R10. Then the mononuclear cells were isolated with LymphoPrep (STEMCELL Technologies Inc) by following the protocol provided by the manufacturer. Mononuclear cells isolated from paired tumor and paratumor tissue were first stained with the LIVE/DEAD® Fixable Aqua Dead Cell Stain Kit (ThermoFisher, UK) before being labelled with conjugated antibodies, with each step of incubation at 4°C for 20 minutes. All samples were acquired on BD LSR Symphony (BD Biosciences) and analyzed using FlowJo™ v.10 software (Tree Star Inc.).

Antibodies used for the surface staining include: BV510-CD16 (3G8; Biolegend; RRID:AB_2562085), BV510-CD56 (HCD56; Biolegend; RRID:AB_2561944), BV510-CD19 (HIB19; Biolegend; RRID:AB_2561668), BV510-CD14 (M5E2; Biolegend; RRID:AB_2561946), BUV395-CD3 (SK7; BD Biosciences; RRID:AB_2744382), PerCP/Cy5.5-CD8 (SK1; BD Biosciences; RRID:AB_2687497), BUV737-CD4 (SK3; BD Biosciences; RRID:AB_2713927), PE-CD56 (MEM-188; Biolegend; RRID:AB_314447), APC-NKG2a (131411; R&D Systems; RRID:AB_356987), PE-Texas Red-CD39 (A1, Biolegend; RRID:AB_2564318), BV785-CD103 (Ber-ACT8; Biolegend; RRID:AB_2734364), BB515-Tim3 (7D3, BD Biosciences; RRID:AB_2744368), BV650-PD-1 (EH12.2H7; Biolegend; RRID:AB_2566362), APC-R700-TIGIT (1G9, BD Biosciences; RRID:AB_2739254), PE/Cy7-CD27 (M-T271; Biolegend; RRID:AB_2562258), BV421-CCR7 (G043H7; Biolegend; RRID:AB_11203894), BV711-CD45RA (HI100; Biolegend; RRID:AB_11218999) and FITC-CD28 (CD28.2; BD Biosciences; RRID:AB_396071). *In vitro* Integrin-β8 staining on CD103⁺ and CD103⁻ CTLs (isolated from tumor tissue of cancer patient) following exposure to target cells at an E:T ratio of 1:10 for 12 hours was performed using APC-integrin beta 8 (416922; R&D Systems; RRID: AB_2044685).

Immunohistochemical analysis

Preparation of immunohistochemical slides was as previously described (28,29). Briefly, adjacent tissue sections of formalin-fixed, paraffin-embedded tumor tissue from five lung cancer patients were stained immunohistochemically for E-Cadherin (NCH-38; Dako, Denmark; RRID:AB_2341210), CD103 (EPR4166(2); AbCAM, UK; RRID:AB_1142856), and CD8 (C8/144B; Agilent Technologies; RRID:AB_2075537) and automated staining was carried out using the Leica BOND-MAX autostainer (Leica Microsystems) following antigen retrieval using Epitope Retrieval Solution 2 (Leica Microsystems). Analysis was conducted using the Visiopharm Integrator System platform made for analyzing digitized serial slides, with the protocol implemented as Analysis Protocol Packages (APP). Several -APPs were designed to quantify slides stained individually with the antibodies following tissue section realignment. Realignment was performed at both large scale and finer detailed level, to get the best match between the three adjacent slides. Region of interest (ROI) was conducted and first auxiliary APP runs were performed using threshold classification that identifies the tissue regions. The second auxiliary APP runs done on the E-Cadherin slides used threshold classification identifying positive and margin regions. ROI was then superimposed on aligned CD8- and CD103-stained slides for subsequent analysis. An HDAB-DAB color deconvolution band was used to detect positively stained cells on CD103 and CD8 slides. To enhance the stained cells, while suppressing the background variation, several pre-processing steps were included. This included the color deconvolution bands were input to a threshold classifier. The thresholding classification method defines a threshold for a given feature and assigns one class to all pixels with a feature value above or equal to that value, and another class for the rest.

The classification rule is defined as:

$$Class(Feature(X,Y)) = \begin{cases} A, & Feature(x,y) \geq T \\ B, & Otherwise \end{cases}$$

where T is the user-selected threshold (cut-off value), A and B are the labels/classes to which the pixel is assigned. For post-processing steps, a method for cell separation which is based on shape and size was used (to exclude the effect of slide preparation). Cell areas that were too small (if a cell was found to be dysregular or deemed as having

cellular membrane damaged) were removed, and we applied an unbiased counting of frames to avoid the cells intersecting with neighboring tile boundaries, which were counted twice (or more). Cells present at 'within' was defined as cells located within the E-Cadherin⁺ regions, cells present at 'clustering' was defined as cells located within 1.5 cm from the E-Cadherin⁺ regions, and cells present at 'distal' was defined as cells located over 1.5 cm from the E-Cadherin⁺ regions.

Statistical analysis

All graph generation and statistical analyses were conducted using GraphPad Prism v.7 software. Unless stated otherwise, data are summarized as median \pm S.E.M. The number of patients used for each *ex vivo* analysis is shown in the figure legends. Each *in vitro* CTL functional assay was replicated three times. Statistically significant differences between two groups were assessed using a two-tailed paired *t*-test, with Wilcoxon adjustments for non-parametrically distributed variables. For comparisons between more than two paired groups of tissues or treatments, one-way ANOVA with Tukey's multiple comparison test was performed. Statistical analysis of the metabolic assays, as well as comparisons between different blocking treatments, were carried out using two-way ANOVA with Tukey's multiple comparison test. All tests were two-sided, and differences were considered as statistically significant as *p*-value <0.05. Data inquisition is upon request.

Results

Cancer-specific CTLs self-regulate CD103 expression

Following initial antigen contact, naïve T cells develop and acquire CD103 expression in the presence of TGF β 1, known to be produced by DCs and Tregs (8-10). However, tumor-infiltrating DCs are dysfunctional in cancer patients (12-14). Thus, it remains unclear how CD103 expression is maintained on matured, differentiated cancer-specific CTLs. Paired CD103⁺ and CD103⁻ cancer-specific CTLs were sorted

and clonally expanded (SSX-2-specific CTLs; NY-ESO-1-specific CTLs) as described in our previous studies (20,21,23)(**Supplementary Fig. S1**). Both paired CD103⁺ and CD103⁻ cancer-specific CTLs had a predominantly late-stage effector memory phenotype (CD28⁻CD27⁻CD45RO⁺CD45RA⁻CCR7⁻) and expressed the standard Tm marker CD69 (**Supplementary Fig. S2A-B**). Each pair of CTLs had the same TCR usage and TCR surface density (**Supplementary Fig. S2C-D**). Specifically, paired CD103⁺ and CD103⁻ SSX-2-specific CTLs used TRAV 8-6 TRAJ 30 and TRBV 6-1 TRBJ 2-7, whereas paired CD103⁺ and CD103⁻ NY-ESO-1-specific CTLs used TRAV 12-2 TRAJ 31 and TRBV 12-4 TRBJ 1-2. The standardization of TCR and phenotype between paired CTLs helps (i) to eliminate other confounding factors that could impact CTLs functions, such as different TCR affinity and recognition strength, and (ii) to ensure any observational changes to the CTL function is due to the action of CD103 on T cells.

As TGFβ1 is known to induce CD103 expression on CTLs (8-10), we therefore assessed the TGFβ1 on CD103⁺ cancer-specific CTLs. Significantly high TGFβ1 was produced by CD103⁺ cancer-specific CTLs but not by the CD103⁻ subset following coculture with peptide-loaded HCT116 cells (**Fig. 1A**). A significant production of TGFβ1 by CD103⁺ CTLs was observed, even after taking into consideration the cytokine production by HCT116 cells (**Fig. 1A**).

Previous studies show that HCT116 do not express NY-ESO-1 and SSX-2 proteins (24-27). In our current study, we confirmed that cancer-specific CTLs did induce IFNγ and TNFα in cocultures with HCT116 cells in the absence of external peptide loading (**Supplementary Fig. S3**). Therefore, HCT116 cells itself did not stimulate SSX-2-specific and NY-ESO-1-specific T-cell responses due to the lack of SSX-2 and NY-ESO-1 expression.

Because the presence of CD103 on cancer-specific CTLs may contribute to self-TGFβ1 production, we next evaluated whether interfering with the interaction of CD103 and its ligand E-Cadherin on HCT116 cells could affect TGFβ1 production. Following anti-CD103 treatment, we found that the TGFβ1 production still remained high (**Fig. 1B**). The TGFβ1 self-producing capacity by CD103⁺ CTLs was validated using

intracellular cytokine staining analysis. The majority of CD103⁺ CTLs expressed intracellular TGFβ1, which was not seen with CD103⁻ CTLs (**Fig. 1C-D**). TGFβ1 was also expressed by CD103⁺ CTLs after treatment with anti-CD3/CD28 in the absence of target cells (**Fig. 1D**). These observations, therefore, suggest that CD103⁺ CTLs independently expressed and produced their own TGFβ1, which is likely responsible for sustaining its CD103 expression.

Because the active form of TGFβ1 was an essential component for CD103 induction, we then assessed whether integrin β8 (known to cleave the inactive form of TGFβ1) was upregulated on TGFβ1⁺CD103⁺ CTLs. TGFβ1⁺CD103⁺ CTLs had significant upregulation of membranous β8 compared to the CD103⁻ CTLs following peptide-loaded target cell exposure for 12 hours (**Fig. 1E-F**). The upregulation of integrin β8 on CD103⁺ CTLs' cell surface likely suggests that this marker may contribute to CD103 expression maintenance on matured T cells by facilitating production of the TGFβ1 active form.

CD103 helps to improve tumor antigen sensitivity of CTLs

It is well-established that human CTA-specific T cells have low affinity TCRs (15, 16). Thus, we next assessed whether CD103 presence on T cells could assist in improving tumor antigen sensitivity and strengthening TCR-mediated effector responses. Following coculture of CTLs with HCT116 cells pre-incubated with various doses of peptides, the CD103⁺ cancer-specific CTLs demonstrated significantly elevated IFNγ responses compared to the CD103⁻ CTLs and was sensitive up to 0.4 μg/mL antigen stimulation (**Fig. 2A**). The reduced IFNγ production by CD103⁺ CTLs following treatment with anti-CD103 (**Fig. 2A**) clearly indicated that CD103 helped to improve tumor antigen sensitivity of cancer-specific CTLs.

CD107a marker is an indicator of degranulation and potential granule-mediated cytotoxic responses of T cells. Therefore, we evaluated whether the enhanced TCR tumor antigen sensitivity affected degranulation by CD103⁺ CTLs. Consistent with the IFNγ response, we observed that CD107a expression was also significantly elevated on CD103⁺ CTLs and was sensitive up to 0.4 μg/mL antigen stimulation (**Fig. 2B**), and

degranulation was impaired following anti-CD103 treatment of CD103⁺ CTLs (**Fig. 2B**). We then assessed whether the enhanced degranulation capacity could improve CD103⁺ CTL anti-tumor cytotoxicity. As expected, significantly higher numbers of HCT116 target cells were killed by CD103⁺ cancer-specific CTLs, even with 0.4 µg/mL antigen stimulation (**Fig. 2C**).

Because E-Cadherin is a known ligand of CD103, we next asked whether their interaction was necessary to improve tumor antigen sensitivity. To do this, we cocultured CD103⁺ CTLs with the E-Cadherin-negative THP-1 cancer cell line. As shown in **Fig. 2D**, CD103⁺ CTLs had significantly reduced degranulation in cocultures with THP-1 cells compared to the E-Cadherin-positive HCT116 cells. We further found that in the presence of THP-1 cells, CD103⁺ CTLs showed significant reduction of target cell killing (**Fig. 2E**). This further confirmed that CD103 and its interaction with E-Cadherin on target cells contributed to enhanced TCR recognition and tumor antigen sensitivity, thus, resulting in enhanced granule-mediated cytotoxicity.

Rapid and accumulating cancer cell killing by CD103⁺ CTLs

We next assessed whether tumor antigen-sensitive CD103⁺ cancer-specific CTLs could perform more efficient single-cell cancer killing. Using live cell imaging, we measured the timing of individual cytotoxic events following CTL exposure to peptide-loaded HCT116 cells. CD103⁺ CTLs initiated significantly faster target cell killing compared to the CD103⁻ CTLs, which required a longer period of time to initiate killing (**Fig. 3A-B; Supplementary Movies S1-S4**), and higher numbers of CD103⁻ CTLs were required to initiate the killing of individual target cells (**Fig. 3A, Supplementary Movie S1-S4**). These observations suggest that the presence of CD103 helps mediate a quicker cytotoxic T-cell response. Indeed, the efficient individual target cell killing by CD103⁺ CTLs became more apparent as early as 4 hours after target cell exposure (**Fig. 3C-D**). The cytotoxic activities of CD103⁺ CTLs resulted in significantly higher HCT116 cell death over a 12-hour time period compared to CD103⁻ CTLs (**Fig. 3E, Supplementary Fig. S4**).

To confirm that the CD103 and E-Cadherin interaction was contributing to the enhanced CTL cytotoxicity, we also cocultured CD103⁺ CTLs with peptide-loaded, E-Cadherin-negative THP-1 cells. No difference in THP-1 cell death following co-culture with either CD103⁺ CTLs or CD103⁻ CTLs was seen across a 12-hour time period (**Supplementary Fig. S5**). Taken together, these observations clearly highlight the importance of CD103 and its interaction with E-Cadherin in elevating CTL antitumor responses.

CD103⁺ cancer-specific CTLs have high energetic potential

Previous studies have highlighted the importance of aerobic glycolysis (glucose oxidation) not only as the major energy source for activated T-cell function, but also as a regulator of cytokine production (30, 31). Thus, we next investigated the metabolic capacity of CD103⁺ cancer-specific CTLs by evaluating their glycolytic activity. CD103⁺ CTLs had significantly higher basal glycolytic rates compared to the CD103⁻ CTLs (**Fig. 4A-B**). CD103⁺ CTLs also showed significantly elevated maximal glycolytic capacity (**Fig. 4A, C**). This suggested that CD103⁺ CTLs could utilize and convert glucose at a faster rate to produce energy, which could potentially be used to induce more efficient and rapid immune responses.

However, in the tumor microenvironment, enhanced glucose consumption by cancer cells is known to deprive TILs of glucose for their cellular functions (32). It is, therefore, vital for CD103⁺ cancer-specific CTLs to be able to efficiently catalyze multiple metabolites, especially during conditions of stress. Therefore, we evaluated the total metabolite consumption capacity of activated CD103⁺ CTLs by assessing the total oxygen consumption rate (OCR) as a measure of the overall T-cell mitochondrial activity. We found that the CD103⁺ CTLs had a significantly higher basal metabolic activity compared to the CD103⁻ CTLs (**Fig. 4D-E**). CD103⁺ CTLs also had a larger spare mitochondrial capacity (**Fig. 4D, F**), suggesting their potential in utilizing various metabolites at higher levels compared to the CD103⁻ CTLs in order to meet energy requirements.

Better homing and localization of CD103⁺ CTLs on E-Cadherin rich tumor cells

Activation of CD103 and its cytoplasmic tail domain in T cells is known to enhance T-cell retention in tumor tissue (33-35). We therefore assessed whether CD103 could mediate better recognition, homing, and retention of T cells to cancer cells. To do this, we initially placed either the CD103⁺ or CD103⁻ cancer-specific CTLs across a transwell barrier, away from HCT116 cells, and allowed any movement to occur within 2 hours period. Within the first hour, the CD103⁺ CTLs migrated in significantly larger numbers across the barrier towards HCT116 cells (**Fig. 5A**). Treatment of the CD103⁺ CTLs with anti-CD103 significantly reduced the number of T cells migrating towards target cells to a level similar to that of the CD103⁻ CTLs (**Fig. 5B**). To validate the necessity of CD103 in T-cell mobility and homing, we exposed CD103⁺ CTLs to E-Cadherin-negative THP-1 cells. No significant difference in the numbers of CD103⁺ CTLs and CD103⁻ CTLs migrating towards THP-1 was found (**Supplementary Fig. S6**). These *in vitro* data indicated the importance of CD103 in the movement and migration of CTLs towards E-Cadherin-positive cancer cells.

In support of our *in vitro* observations, we carried out *ex vivo* immunohistochemistry on cross-sectional tumor tissues from five lung cancer patients. We found that CD103⁺CD8⁺ TILs localized at the E-cadherin-rich tumor islets, whereas CD103⁻CD8⁺ TILs were mainly in the E-Cadherin-absent tumor regions. CD103⁺CD8⁺ TILs significantly clustered around, as well as within, the E-cadherin rich tumor islets at a significantly higher frequency and density (**Fig. 6A-B**). In contrast, the CD103⁻CD8⁺ TILs were much denser, distal from the E-Cadherin⁺ tumor islets (**Fig. 6A-B**). Altogether, these observations highlighted that CD103⁺ CTLs had better homing and clustering capacity to cancer cells expressing E-Cadherin.

Prolonged exposure of CD103⁺ T cells to cancer contributes to T-cell death

It was previously shown that TILs co-expressing CD103 and CD39 are tumor-reactive TILs, with increased inhibitory receptor expression (19). However, it remains unclear whether CD103⁺ TILs have different subpopulations with distinctive exhaustion immunophenotypes. We first categorized *ex vivo* TILs derived from paired tumor and

paratumor tissues from five lung cancer patients according to their CD103 and CD39 expression. Only the CD103⁺ TILs derived from the tumor expressed high CD39 (CD39^{high}) but not the CD103⁺ T cells derived from the paratumor tissue (**Fig. 7A**). In contrast, the CD103⁺CD39^{lo} T-cell subpopulation could be found in both paired tissue samples (**Fig. 7A**). This indicated the presence of multiple CD103⁺ TIL subpopulations and suggests potential differences in their immunophenotype. Only the CD103⁺CD39^{high} TIL subpopulation had higher expression of PD-1, Tim3, and TIGIT (**Fig. 7B, Supplementary Fig. S7**). This subpopulation had a significantly higher frequency of PD-1⁺Tim3⁺TIGIT⁺ cells (**Fig. 7C**). In contrast, the CD103⁺CD39^{low} TIL subpopulation lacked Tim3 and NKG2A expression, with only 40% PD-1⁺TIGIT⁺ cells (**Fig. 7D**). These observations, therefore, suggested that only some CD103⁺ TILs acquired Tim3 expression and had high co-expression of different inhibitory receptors.

Upregulation of inhibitory receptors on TILs is one of the marks of T-cell activation and exhaustion. To further assess whether prolonged antigen exposure of CD103⁺ CTLs in cancer could impair T-cell survival, we cocultured CD103⁺ CTLs with HCT116 cells for a 12-hour period *in vitro*. We found that prolonged cancer exposure resulted in significantly increased CD103⁺ CTLs expressing activated caspase-3 compared to the CD103⁻ CTLs (**Fig. 7E**). Because activated caspase-3 presence is known to be an indicator of cellular apoptosis, we evaluated CD103⁺ CTL cell death after prolonged cancer exposure. As expected, a significantly higher number of CD103⁺ T cell death was observed following prolonged cancer exposure compared to CD103⁻ T-cell death (**Fig. 7F**). These observations suggest that CD103⁺ CTLs were more prone to apoptosis following prolonged cancer exposure.

Discussion

The association of CD103⁺ TIL enrichment with improved clinical outcomes in cancer patients (3, 4) highlights the need to have a clear and comprehensive understanding of the CD103-mediated characteristics of cancer-specific CTLs and their implications for future immunotherapies. We demonstrated that mature differentiated CD103⁺ cancer-specific CTLs could self-regulate their CD103 expression by producing

activated TGF β 1, without needing to rely on external cues from other TGF β 1-producing cells. We further showed that the presence of CD103 improved TCR antigen sensitivity and enabled faster cancer recognition and more rapid and efficient cancer cell killing. CD103⁺ CTLs were also found to have an elevated energetic potential and faster migration capacity. However, our data also demonstrated that CD103⁺ cancer-specific CTLs are more susceptible to apoptosis following prolonged cancer exposure.

It is well established that DCs, and most likely Tregs, are the main players in producing TGF β 1 for inducing CD103 expression on developing CTLs (8-10). Both TGF β 1 and antigen exposure are required to induce a CD103 tissue residential T-cell signature (36, 37). We found that mature CD103⁺ cancer-specific CTLs, but not CD103⁻ CTLs, could self-produce activated TGF β 1 to continually sustain prolonged CD103 expression, without needing to rely on other external TGF β 1-producing cells. The self-regulation of CD103 maintenance indicates a possibly unique subset of cancer-specific T cells that could be present in the tumor microenvironment with unique and effective antitumor immune properties. However, the frequency of this CD103⁺TGF β 1⁺ self-regulatory, cytotoxic T-cell population and its importance, especially during cancer growth, merits further investigation.

Our *in vitro* data showed that CD103⁺ cancer-specific CTLs had higher energy potential compared to CD103⁻ CTLs. However, in the tumor microenvironment, enhanced glucose consumption by cancer cells can deprive TILs of the glucose needed for proper T-cell function (32). This therefore suggests that CD103⁺ CTLs need to be able to utilize different metabolites to meet their high energy demand. Previous work by Kupper and colleagues has highlighted the capacity of virus-specific Trm cells to take up exogenous free fatty acids and this accounts for the long-term survival of T cells and further helps in mediating protective immunity in virus-infected tissues (38). In light of this, it merits further investigation on whether CD103⁺ cancer-specific Trm cells are able to utilize a variety of metabolites and how this impacts their effector function and survival, especially in the glucose-deprived tumor microenvironment.

It is well-established that human cancer-specific T cells have low-affinity TCRs and, therefore, have less efficient TCR-mediated activating signaling (15). Because

CD103 is known to accumulate in the immunological synapse (18), it is likely that increasing CD103 and E-Cadherin interactions could strengthen the affinity of TCR binding and, therefore, increase the sensitive engagement with the tumor antigen/MHC complex on cancer cells. We demonstrated that the CD103 and E-Cadherin interaction improved the efficiency of TCR-mediated effector responses by CD103⁺ CTLs. In addition to improve TCR sensitivity, it is also likely that CD103 could assist in improving TCR-mediated signaling. Previous work has highlighted that CD103 could enhance the phosphorylation of two key downstream proteins of TCR signaling, ERK1/2 and PLC γ 1 (18). Therefore, the specific mechanisms of CD103 in mediating TCR downstream signaling necessitates further investigation.

Co-expression of CD103 and CD39 has been demonstrated to mark tumor-reactive TILs (19). A study also indicates that regulation of TILs in tumor tissue can lead to competition between anti-tumoral Trm activity and pro-tumoral exhaustion activity (39). Here, we demonstrated varying subpopulations of CD103⁺ TILs that are present in tumor microenvironment and that only the CD39^{high}CD103⁺ TIL subpopulation co-expressed multiple inhibitory receptors. Our data also showed that prolonged exposure of CD103⁺ CTLs to cancer could result in more T-cell apoptosis, which goes hand-in-hand with our previous finding that the overall frequency of CD103⁺ TILs diminishes as tumor size progresses (40). Based on our current study, the CD103⁺CD39^{low} TIL subpopulation as an alternative tumor-reactive subpopulation could be a critical Trm population that can be improved using novel tissue-localized immunotherapy strategies. In summary, our data shed light on the working and characteristics of CD103⁺ cancer-specific CTLs, which could provide significant insights for future design of novel tissue-localized antitumor T-cell immunotherapies.

Acknowledgements: We thank the Wolfson Imaging Centre Oxford (WIMM, Oxford) for providing microscope facility support and sequencing of the TCR by John Frankland and Timothy Frankland (Sequencing Facility, WIMM, Oxford). We acknowledge the contribution to this study made by the Oxford Centre for Histopathology Research and

the Oxford Radcliffe Biobank, which are supported by the NIHR Oxford Biomedical Research Centre, Sally Ann-Clark (WIMM, Oxford) with flow cytometry help, Marahaini Musa (Dept. Oncology, UK; USM, Malaysia) for assistance, Guihai Liu and Bella Bu for mRNA extraction and Clare Hardman and Janina Nahler for advice on transwell migration assay. We acknowledge the editing support of Life Science Editors. The views expressed are those of the author(s) and not necessarily of the National Health Service (NHS), the NIHR or the Department of Health, UK.

Author contributions:

Conception and design: T. Dong, M. Abd Hamid and Y. Peng

Development of methodology: M. Abd Hamid, H. Colin-York, N. Khalid-Alham and Y. Peng

Acquisition of data (e.g., provided cells, acquired and managed patients, provided facility, etc): J. Chen, C. Waugh, D. Maldonado-Perez, E. Bowes and C. Verrill

Analysis and interpretation of data (e.g., statistical analysis, biostatistics, computational analysis): M. Abd Hamid, H. Colin-York, N. Khalid-Alham, S. Rosendo-Machado, M. Friztsche, Y. Peng and T. Dong

Study supervision: Y. Peng and T. Dong

Writing, review and/or revision of the manuscript: M. Abd Hamid, H. Colin-York, V. Cerundolo, C. Conlon, M. Friztsche, Y. Peng and T. Dong.

Other (oversight of the REC approval (ORB) and team under which tissue research was conducted): C. Verrill

References

1. Mackay LK, Rahimpour A, Ma JZ, Collins N, Stock AT, Hafon ML, et al. The developmental pathway for CD103(+)CD8+ tissue-resident memory T cells of skin. *Nat Immunol.* 2013;14(12):1294-301.
2. Piet B, de Bree GJ, Smids-Dierdorp BS, van der Loos CM, Remmerswaal EB, von der Thusen JH, et al. CD8(+) T cells with an intraepithelial phenotype upregulate cytotoxic function upon influenza infection in human lung. *J Clin Invest.* 2011;121(6):2254-63.
3. Djenidi F, Adam J, Goubar A, Durgeau A, Meurice G, de Montpreville V, et al. CD8+CD103+ tumor-infiltrating lymphocytes are tumor-specific tissue-resident memory T cells and a prognostic factor for survival in lung cancer patients. *J Immunol.* 2015;194(7):3475-86.
4. Ganesan AP, Clarke J, Wood O, Garrido-Martin EM, Chee SJ, Mellows T, et al. Tissue-resident memory features are linked to the magnitude of cytotoxic T cell responses in human lung cancer. *Nat Immunol.* 2017;18(8):940-50.
5. Malik BT, Byrne KT, Vella JL, Zhang P, Shabaneh TB, Steinberg SM, et al. Resident memory T cells in the skin mediate durable immunity to melanoma. *Sci Immunol.* 2017;2(10).
6. Wang B, Wu S, Zeng H, Liu Z, Dong W, He W, et al. CD103+ Tumor Infiltrating Lymphocytes Predict a Favorable Prognosis in Urothelial Cell Carcinoma of the Bladder. *J Urol.* 2015;194(2):556-62.
7. Quinn E, Hawkins N, Yip YL, Suter C, Ward R. CD103+ intraepithelial lymphocytes--a unique population in microsatellite unstable sporadic colorectal cancer. *Eur J Cancer.* 2003;39(4):469-75.
8. Yu CI, Becker C, Wang Y, Marches F, Helft J, Leboeuf M, et al. Human CD1c+ dendritic cells drive the differentiation of CD103+ CD8+ mucosal effector T cells via the cytokine TGF-beta. *Immunity.* 2013;38(4):818-30.

9. Enamorado M, Iborra S, Priego E, Cueto FJ, Quintana JA, Martinez-Cano S, et al. Enhanced anti-tumour immunity requires the interplay between resident and circulating memory CD8(+) T cells. *Nat Commun.* 2017;8:16073.
10. Graham JB, Da Costa A, Lund JM. Regulatory T cells shape the resident memory T cell response to virus infection in the tissues. *J Immunol.* 2014;192(2):683-90.
11. Nizard M, Roussel H, Diniz MO, Karaki S, Tran T, Voron T, et al. Induction of resident memory T cells enhances the efficacy of cancer vaccine. *Nat Commun.* 2017;8:15221.
12. Herber DL, Cao W, Nefedova Y, Novitskiy SV, Nagaraj S, Tyurin VA, et al. Lipid accumulation and dendritic cell dysfunction in cancer. *Nat Med.* 2010;16(8):880-6.
13. Cubillos-Ruiz JR, Silberman PC, Rutkowski MR, Chopra S, Perales-Puchalt A, Song M, et al. ER Stress Sensor XBP1 Controls Anti-tumor Immunity by Disrupting Dendritic Cell Homeostasis. *Cell.* 2015;161(7):1527-38.
14. Karyampudi L, Lamichhane P, Krempski J, Kalli KR, Behrens MD, Vargas DM, et al. PD-1 Blunts the Function of Ovarian Tumor-Infiltrating Dendritic Cells by Inactivating NF-kappaB. *Cancer Res.* 2016;76(2):239-50.
15. Thomas S, Xue SA, Bangham CR, Jakobsen BK, Morris EC, Stauss HJ. Human T cells expressing affinity-matured TCR display accelerated responses but fail to recognize low density of MHC-peptide antigen. *Blood.* 2011;118(2):319-29.
16. Aleksic M, Liddy N, Molloy PE, Pumphrey N, Vuidepot A, Chang KM, et al. Different affinity windows for virus and cancer-specific T-cell receptors: implications for therapeutic strategies. *Eur J Immunol.* 2012;42(12):3174-9.
17. Le Floch A, Jalil A, Vergnon I, Le Maux Chansac B, Lazar V, Bismuth G, et al. Alpha E beta 7 integrin interaction with E-cadherin promotes antitumor CTL activity by triggering lytic granule polarization and exocytosis. *J Exp Med.* 2007;204(3):559-70.
18. Le Floch A, Jalil A, Franciszkiewicz K, Validire P, Vergnon I, Mami-Chouaib F. Minimal engagement of CD103 on cytotoxic T lymphocytes with an E-cadherin-Fc molecule triggers lytic granule polarization via a phospholipase Cgamma-dependent pathway. *Cancer Res.* 2011;71(2):328-38.

19. Duhén T, Duhén R, Montler R, Moses J, Moudgil T, de Miranda NF, et al. Co-expression of CD39 and CD103 identifies tumor-reactive CD8 T cells in human solid tumors. *Nat Commun.* 2018;9(1):2724.
20. Zhang C, Peng Y, Hublitz P, Zhang H, Dong T. Genetic abrogation of immune checkpoints in antigen-specific cytotoxic T-lymphocyte as a potential alternative to blockade immunotherapy. *Sci Rep.* 2018;8(1):5549.
21. Abd Hamid M, Wang RZ, Yao X, Fan P, Li X, Chang XM, et al. Enriched HLA-E and CD94/NKG2A Interaction Limits Antitumor CD8(+) Tumor-Infiltrating T Lymphocyte Responses. *Cancer Immunol Res.* 2019;7(8):1293-306.
22. Dong T, Stewart-Jones G, Chen N, Easterbrook P, Xu X, Papagno L, et al. HIV-specific cytotoxic T cells from long-term survivors select a unique T cell receptor. *J Exp Med.* 2004;200(12):1547-57.
23. Chen JL, Dawoodji A, Tarlton A, Gnjjatic S, Tajar A, Karydis I, et al. NY-ESO-1 specific antibody and cellular responses in melanoma patients primed with NY-ESO-1 protein in ISCOMATRIX and boosted with recombinant NY-ESO-1 fowlpox virus. *Int J Cancer.* 2015;136(6):E590-601.
24. Purbhoo MA, Sutton DH, Brewer JE, Mullings RE, Hill ME, Mahon TM, et al. Quantifying and imaging NY-ESO-1/LAGE-1-derived epitopes on tumor cells using high affinity T cell receptors. *J Immunol.* 2006;176(12):7308-16.
25. Gjerstorff MF, Relster MM, Greve KB, Moeller JB, Elias D, Lindgreen JN, et al. SSX2 is a novel DNA-binding protein that antagonizes polycomb group body formation and gene repression. *Nucleic Acids Res.* 2014;42(18):11433-46.
26. Greve KB, Pohl M, Olsen KE, Nielsen O, Ditzel HJ, Gjerstorff MF. SSX2-4 expression in early-stage non-small cell lung cancer. *Tissue Antigens.* 2014;83(5):344-9.
27. Saias L, Gomes A, Cazales M, Ducommun B, Lobjois V. Cell-Cell Adhesion and Cytoskeleton Tension Oppose Each Other in Regulating Tumor Cell Aggregation. *Cancer Res.* 2015;75(12):2426-33.
28. Freedman JD, Duffy MR, Lei-Rossmann J, Muntzer A, Scott EM, Hagel J, et al. An Oncolytic Virus Expressing a T-cell Engager Simultaneously Targets Cancer and Immunosuppressive Stromal Cells. *Cancer Res.* 2018;78(24):6852-65.

29. Pell R, Oien K, Robinson M, Pitman H, Rajpoot N, Rittscher J, et al. The use of digital pathology and image analysis in clinical trials. *J Pathol Clin Res*. 2019;5(2):81-90.
30. Chang CH, Curtis JD, Maggi LB, Jr., Faubert B, Villarino AV, O'Sullivan D, et al. Posttranscriptional control of T cell effector function by aerobic glycolysis. *Cell*. 2013;153(6):1239-51.
31. Menk AV, Scharping NE, Moreci RS, Zeng X, Guy C, Salvatore S, et al. Early TCR Signaling Induces Rapid Aerobic Glycolysis Enabling Distinct Acute T Cell Effector Functions. *Cell Rep*. 2018;22(6):1509-21.
32. Chang CH, Qiu J, O'Sullivan D, Buck MD, Noguchi T, Curtis JD, et al. Metabolic Competition in the Tumor Microenvironment Is a Driver of Cancer Progression. *Cell*. 2015;162(6):1229-41.
33. Boutet M, Gauthier L, Leclerc M, Gros G, de Montpreville V, Theret N, et al. TGFbeta Signaling Intersects with CD103 Integrin Signaling to Promote T-Lymphocyte Accumulation and Antitumor Activity in the Lung Tumor Microenvironment. *Cancer Res*. 2016;76(7):1757-69.
34. Gauthier L, Corgnac S, Boutet M, Gros G, Validire P, Bismuth G, et al. Paxillin Binding to the Cytoplasmic Domain of CD103 Promotes Cell Adhesion and Effector Functions for CD8(+) Resident Memory T Cells in Tumors. *Cancer Res*. 2017;77(24):7072-82.
35. Sathaliyawala T, Kubota M, Yudanin N, Turner D, Camp P, Thome JJ, et al. Distribution and compartmentalization of human circulating and tissue-resident memory T cell subsets. *Immunity*. 2013;38(1):187-97.
36. Ling KL, Dulphy N, Bahl P, Salio M, Maskell K, Piris J, et al. Modulation of CD103 expression on human colon carcinoma-specific CTL. *J Immunol*. 2007;178(5):2908-15.
37. Pallett LJ, Davies J, Colbeck EJ, Robertson F, Hansi N, Easom NJW, et al. IL-2(high) tissue-resident T cells in the human liver: Sentinels for hepatotropic infection. *J Exp Med*. 2017;214(6):1567-80.
38. Pan Y, Tian T, Park CO, Lofftus SY, Mei S, Liu X, et al. Survival of tissue-resident memory T cells requires exogenous lipid uptake and metabolism. *Nature*. 2017;543(7644):252-6.

39. O'Brien SM, Klampatsa A, Thompson JC, Martinez MC, Hwang WT, Rao AS, et al. Function of Human Tumor-Infiltrating Lymphocytes in Early-Stage Non-Small Cell Lung Cancer. *Cancer Immunol Res.* 2019;7(6):896-909.
40. Abd Hamid M, Wang RZ, Yao X, Fan P, Li X, Chang XM, et al. Enriched HLA-E and CD94/NKG2A interaction limits antitumor CD8⁺ tumor-infiltrating T lymphocyte responses. *Cancer Immunol Res.* 2019.

Figure titles and legends

Figure 1. TGFβ1 self-dependency of CD103⁺ cancer-specific T cells. **(A)** TGFβ1 production by either CD103⁺ or CD103⁻ T cells following coculture with HCT116 cells and 1μM antigen or HCT116 cells alone (N, number of repeats=3). **(B)** TGFβ1 production by either CD103⁺ or CD103⁻ T cells following coculture with HCT116 cells with either no treatment, isotype treatment, or anti-CD103 treatment. SSX-2-specific T-cell clones (*left*) and NY-ESO-1-specific T-cell clones (*right*)(N, number of repeats=3). **(C)** Representative flow cytometry dot plots of TGFβ1-expressing CD103⁺ or CD103⁻ CD8⁺ cells specific for SSX-2 following coculture with HCT116 and 1μM antigen (N, number of repeats=3). **(D)** Proportion of TGFβ1⁺ CD103⁺ or CD103⁻ T cells following coculture with HCT116 cell and 1μM antigen or anti-CD3/CD28 (N, number of repeats=3). **(E)** Flow cytometry plots of membranous TGFβ1 and membranous β8 expression on either CD103⁺ or CD103⁻ T cells, at 2, 6, and 12 hours post coculture with 1 μM SSX-2 antigen-stimulated HCT116 cells (N, number of repeats=3). **(F)** Frequency of β8⁺CD103⁺ or CD103⁻ T cells post coculture with 1 μM SSX-2 antigen-stimulated HCT116 cells across 12 hours (N, number of repeats n=3). Data presented as median±S.E.M. *p-value<0.05; **p-values<0.01; ***p-values<0.001; ns, not significant. P-values were calculated using either one-way ANOVA with Tukey post hoc analysis or paired student t-test with Wilcoxon adjustments.

Figure 2. Tumor antigen sensitivity of CD103⁺ cancer-specific T cells. Proportion of CD103⁺ **(A)** IFNγ⁺ T cells and **(B)** CD107a⁺ T cells with either anti-CD103 blocking treatment, isotype control treatment, or no treatment following coculture with HCT116 cells at five different concentrations of antigen. SSX-2 (*left*) and NY-ESO-1 (*right*)

CD103⁻ T cells with no treatment also shown (N, number of repeats=3). **(C)** Proportion of lysed HCT116 cancer cells following coculture with either CD103⁺ T cells left untreated or treated with anti-CD103 or isotype at five different antigen concentrations. CD103⁻ T cells with no treatment also shown (N, number of repeats=3). **(D)** Proportion of CD103⁺CD107a⁺ SSX-2-specific T cells following either coculture with E-Cadherin⁺ HCT116 cells or E-Cadherin⁻ THP-1 cells at five different concentrations of antigen (N, number of repeats=3). **(E)** Proportion of cancer cell death following either coculture with E-Cadherin⁺ HCT116 cells or E-Cadherin⁻ THP-1 cells at five different concentrations of antigen. (A-C), data represented as median±S.E.M. *p-value<0.05; **p-values<0.01; ***p-values<0.001; ns, not significant. P-values were calculated using two-way ANOVA with Tukey post hoc analysis.

Figure 3. Mechanism of CD103⁺ cancer-specific T-cell cytotoxicity. **(A)** Confocal imaging time-lapse of 1 µg SSX-2 antigen-loaded HCT116 cancer cells cocultured either CD103⁺ (*top*) or CD103⁻ (*bottom*) SSX-2-specific T cells labelled with flou4-AM for calcium staining. Close-up images showing brightfield (*top*), flou4-AM stain (*middle*), and merged (*bottom*). Flou4-AM calcium staining shown in red. Scale bar: 10 µm, Blue dotted box indicates zoomed imaged area at magnification of 25X. **(B)** Amount of time (in seconds) required for first instance of 1 µg SSX-2 antigen-loaded HCT116 cancer cells cocultured either CD103⁺ (*top*) or CD103⁻ (*bottom*) SSX-2-specific T cells. N₁, number of events collected for CD103⁺ T cells: 29; N₂, number of events collected for CD103⁻ T cells: 29 (N, number of repeats=3; at 95% percentile). **(C)** Confocal imaging time-lapse 1 µg SSX-2 antigen-loaded HCT116 cancer cells cocultured either CD103⁺ (*top*) or CD103⁻ (*bottom*) SSX-2-specific T cells labelled with Annexin V. Close-up images showing brightfield (*top*), Annexin V (*middle*), and merged (*bottom*) at 3,4,5,6,9,12 hours after coculture. Annexin V staining shown in blue. Scale bar: 10 µm. Blue dotted box indicates zoomed imaged area, at magnification of 25X. **(D)** Normalized annexin V intensity representing HCT116 cell death across a 12-hour time period following 1 µg SSX-2 antigen-loaded of HCT116, and cocultured either CD103⁺ (*top*) or CD103⁻ (*bottom*) SSX-2-specific T cells A close-up detailing 2–8 hours coculture (N, number of repeats=3) is also shown. **(E)** Percentage of HCT116 cell death across a 12-hour time period following 1 µg SSX-2 antigen-loaded of HCT116, and cocultured

either CD103⁺ (*top*) or CD103⁻ (*bottom*) SSX-2-specific T cells (N, number of repeats=3). Data represented as median±S.E.M. *p-value<0.05; **p-values<0.01; ***p-values<0.001; ns, not significant. P-values were calculated using either paired student t-test with Wilcoxon adjustments, one-way or two-way ANOVA with Tukey post hoc analysis.

Figure 4. Metabolic activities of CD103⁺ cancer-specific T cells. (A) The extracellular acidification rates (ECAR) of antigen-stimulated CD103⁺ or CD103⁻ T cells across an 80-minute period. SSX-2 (*left*) and NY-ESO-1 (*right*)(N, number of repeats=3). Injection of glucose, oligomycin, and 2-DG into cells are indicated. The ECAR of (B) basal glycolytic capacity and (C) the maximal glycolytic capacity of antigen-stimulated CD103⁺ or CD103⁻ T cells (N, number of repeats=3). (D) The oxygen consumption rates (OCR) of antigen-stimulated CD103⁺ or CD103⁻ T cells across an 80-minute period. SSX-2 (*left*) and NY-ESO-1 (*right*)(N, number of repeats=3). Injection of oligomycin, FCCP, and rotenone/antimycin A into cells are indicated. The OCR at (E) basal respiration stage and (F) the spare respiratory capacity of antigen-stimulated CD103⁺ or CD103⁻ T cells (N, number of repeats=3). Data represented as median±S.E.M. *p-value<0.05; **p-values<0.01; ***p-values<0.001; ns, not significant. P-values were calculated using either paired student t-test with Wilcoxon adjustments, one-way or two-way ANOVA with Tukey post hoc analysis.

Figure 5. CD103 expression on T cells enables faster migration and homing. (A) The number of CD103⁺ or CD103⁻ SSX-2-specific T cells that migrated across a transwell membrane towards HCT116 cells, over a time period of 2 hours, at E:T ratio of 1:4. SSX-2-specific T cell clones shown on the *left* and NY-ESO-1-specific T clones shown on the *right*. (N, number of repeats=3). (B) The number of CD103⁺ or CD103⁻ T cells that migrated across a transwell membrane after 60 minutes with or without anti-CD103 blocking treatment. SSX-2-specific T cell clones shown on the *left* and NY-ESO-1-specific T clones shown on the *right* (N, number of repeats=3). Data represented as median±S.E.M. *p-value<0.05; **p-values<0.01; ***p-values<0.001; ns, not significant. P-values were calculated using either one-way or two-way ANOVA with Tukey post hoc analysis.

Figure 6. CD103⁺ CD8⁺ TILs localize on E-Cadherin rich tumors. (A) Proportion of CD103⁺CD8⁺ T cells (*left*) or CD103⁻CD8⁺ T cells (*right*) present either within, clustering around, or distal of E-cadherin⁺ cells. (N, number of patients=5; at 95% percentile). **(B)** Density (by μm^2) of CD103⁺CD8⁺ T cells (*left*) or CD103⁻CD8⁺ stained cells (*right*) present either within, clustering around, or distal of E-cadherin⁺ cells (N, number of patients=5). Data represented as median \pm S.E.M *p-value<0.05; **p-values<0.01; ***p-values<0.001; ns, not significant. P-values were calculated using one-way ANOVA with Tukey post hoc analysis.

Figure 7. Ex vivo CD103⁺ TILs phenotype and in vitro analysis of T cell death. (A) Representative flow cytometry contour plots of CD39 and CD103 expression on total CD8⁺ TILs derived from either tumor or paratumor tissues (*left and middle*), with graph showing frequency of CD8⁺ TILs co-expressing CD39 and CD103 across five different lung cancer patients (N, number of patients=5, at 95% percentile). **(B)** Representative tSNE plots identifying total CD3⁺, CD8⁺, and CD4⁺ TILs (*top*); CD103⁺CD39^{high}, CD103⁺CD39^{low}, CD103⁺CD39⁻, and total CD103⁻CD8⁺ TILs (*middle*); and PD-1⁻, Tim3⁻, TIGIT⁻, and NKG2A-expressing TILs. **(C)** Proportion of PD1⁺TIGIT⁺Tim3⁺NKG2A⁻ cells in CD103⁺CD39^{high}, CD103⁺CD39^{low}, CD103⁺CD39⁻, or total CD8⁺ TILs derived from paired tumor and paratumor (N, number of patients=5; at 95% percentile). **(D)** Proportion of PD1⁺TIGIT⁺Tim3⁻NKG2A⁻ cells in CD103⁺CD39^{high}, CD103⁺CD39^{low}, CD103⁺CD39⁻, or total CD8⁺ TILs derived from paired tumor and paratumor (N, number of patients=5, at 95% percentile). The proportion of **(E)** activated caspase-3⁺ T-cells and **(F)** T-cell death following coculture with HCT116 (that was loaded with 1 μg SSX-2 antigen) across a time period of 12 hours (N, number of repeats=3). In A, C, D, E, and F), data represented as median \pm S.E.M. *p-value<0.05; **p-values<0.01; ***p-values<0.001; ns, not significant. P-values were calculated using either one-way or two-way ANOVA with Tukey post hoc analysis.

Figure 1

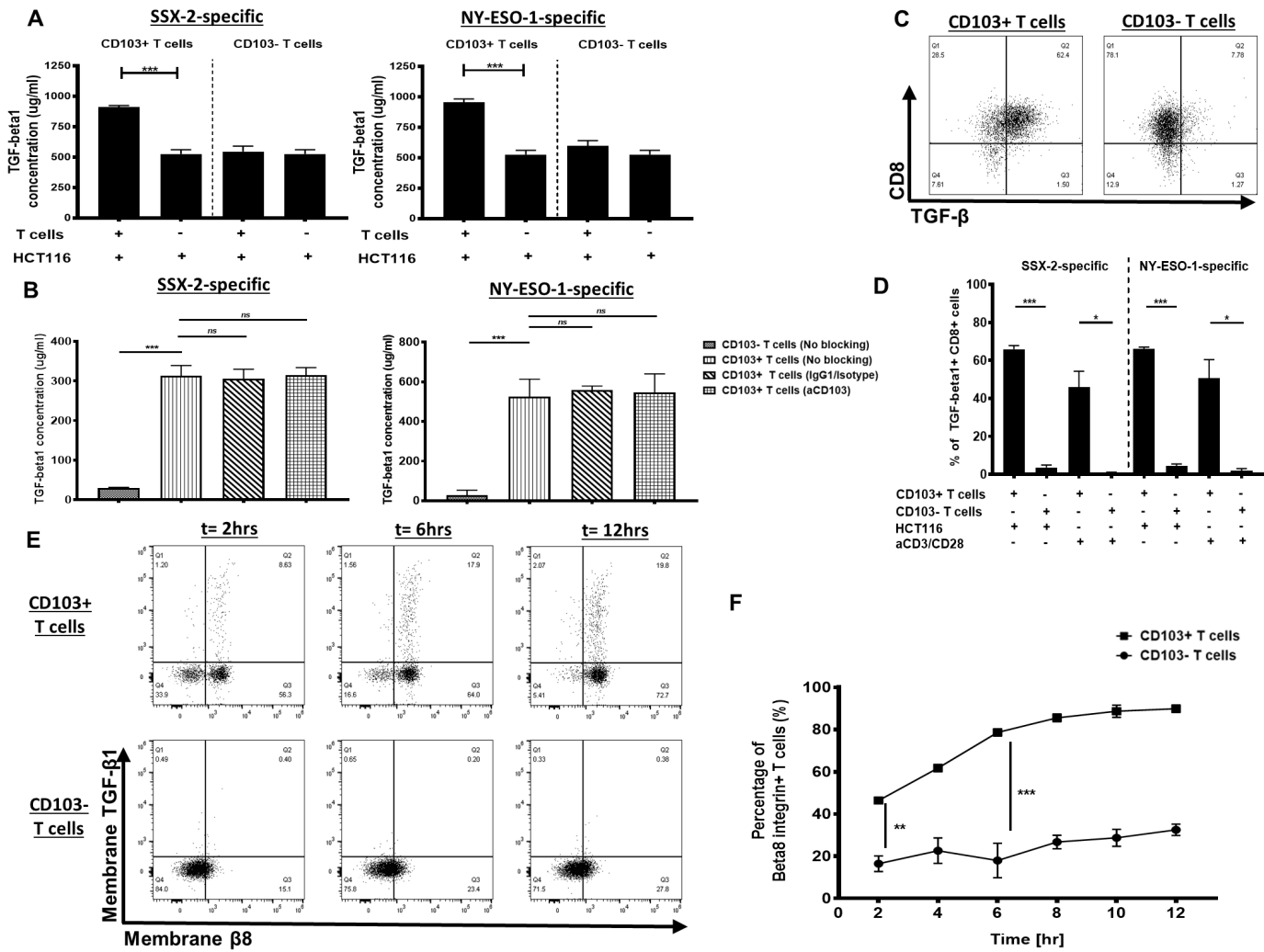


Figure 2

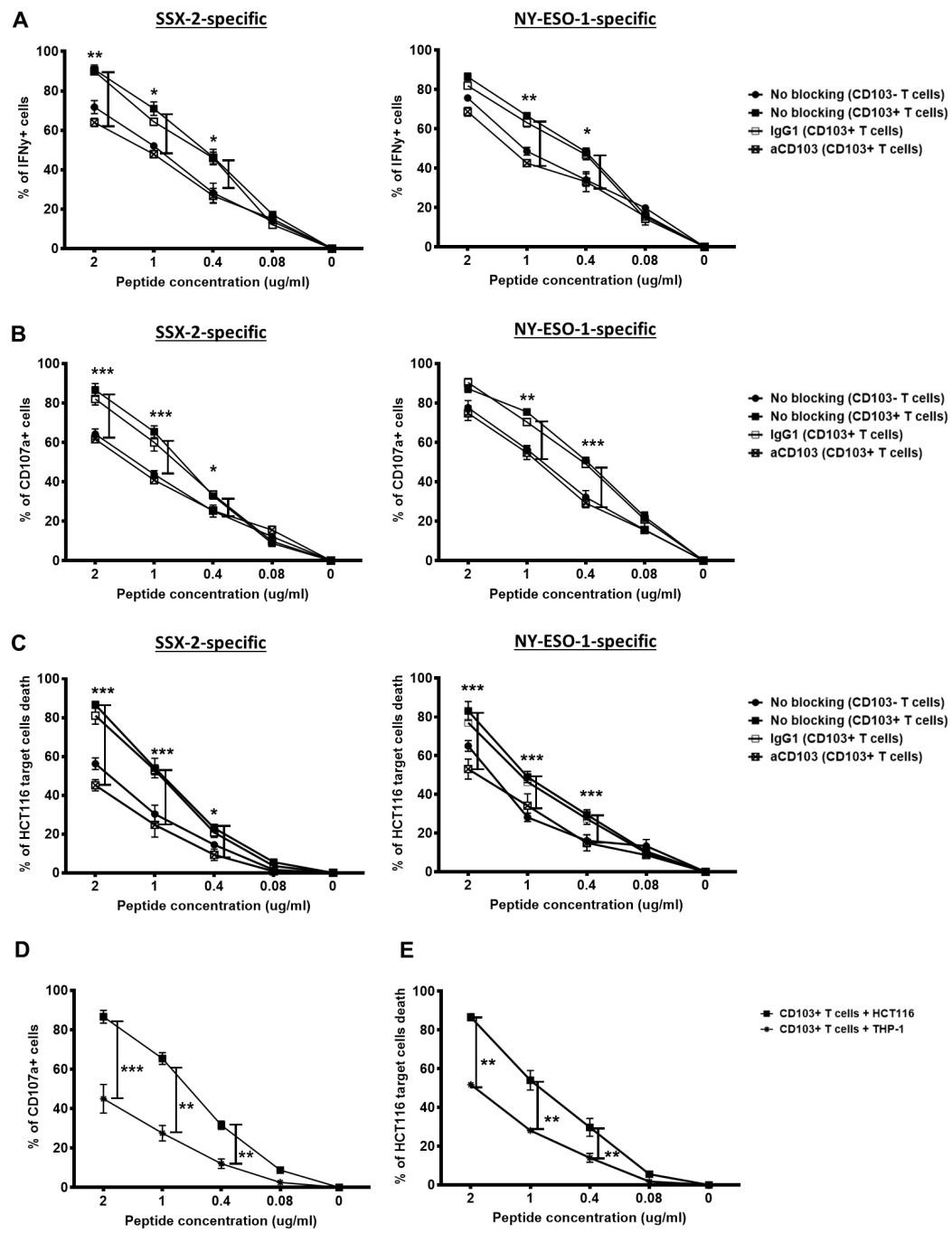


Figure 3

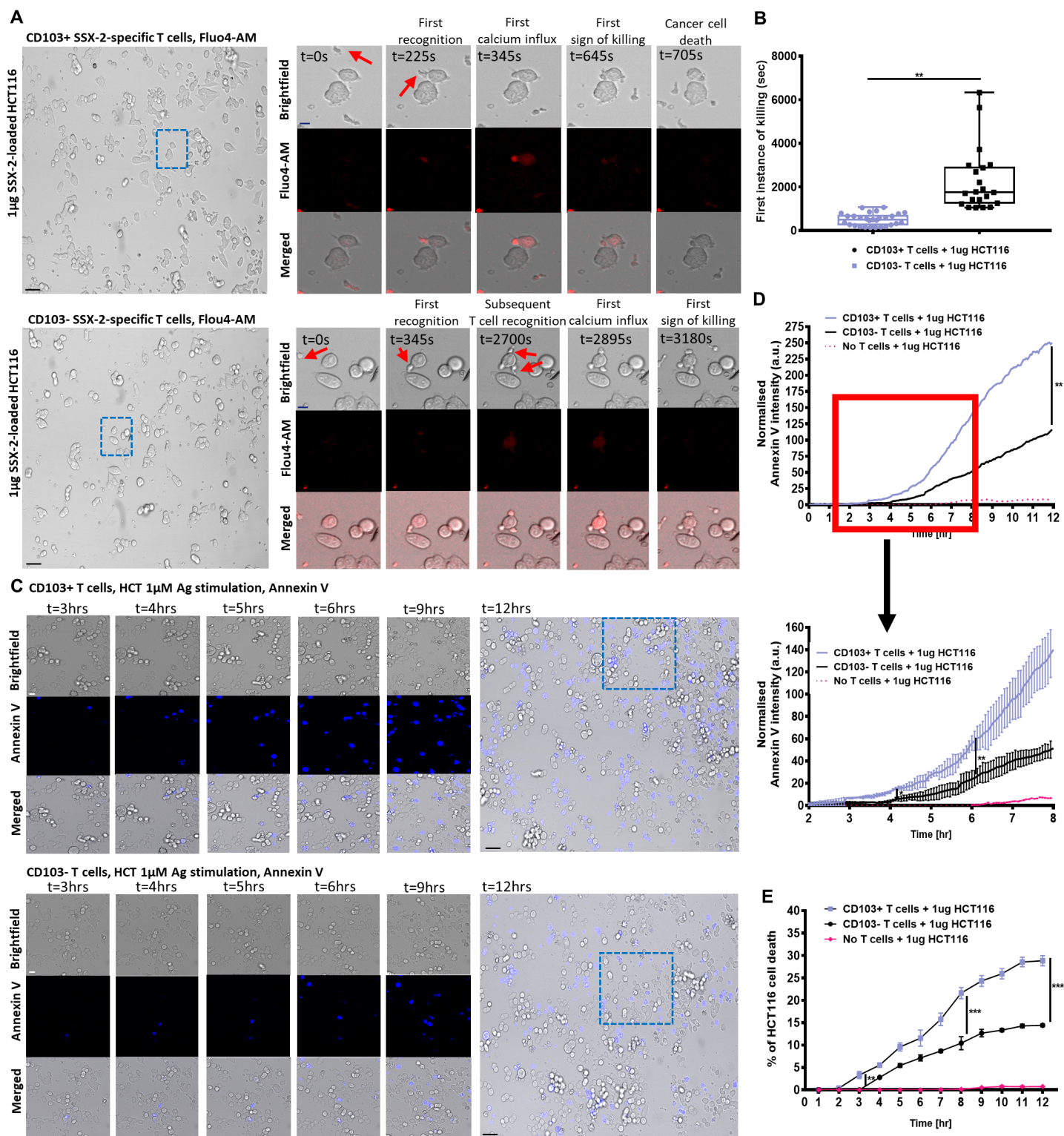


Figure 4

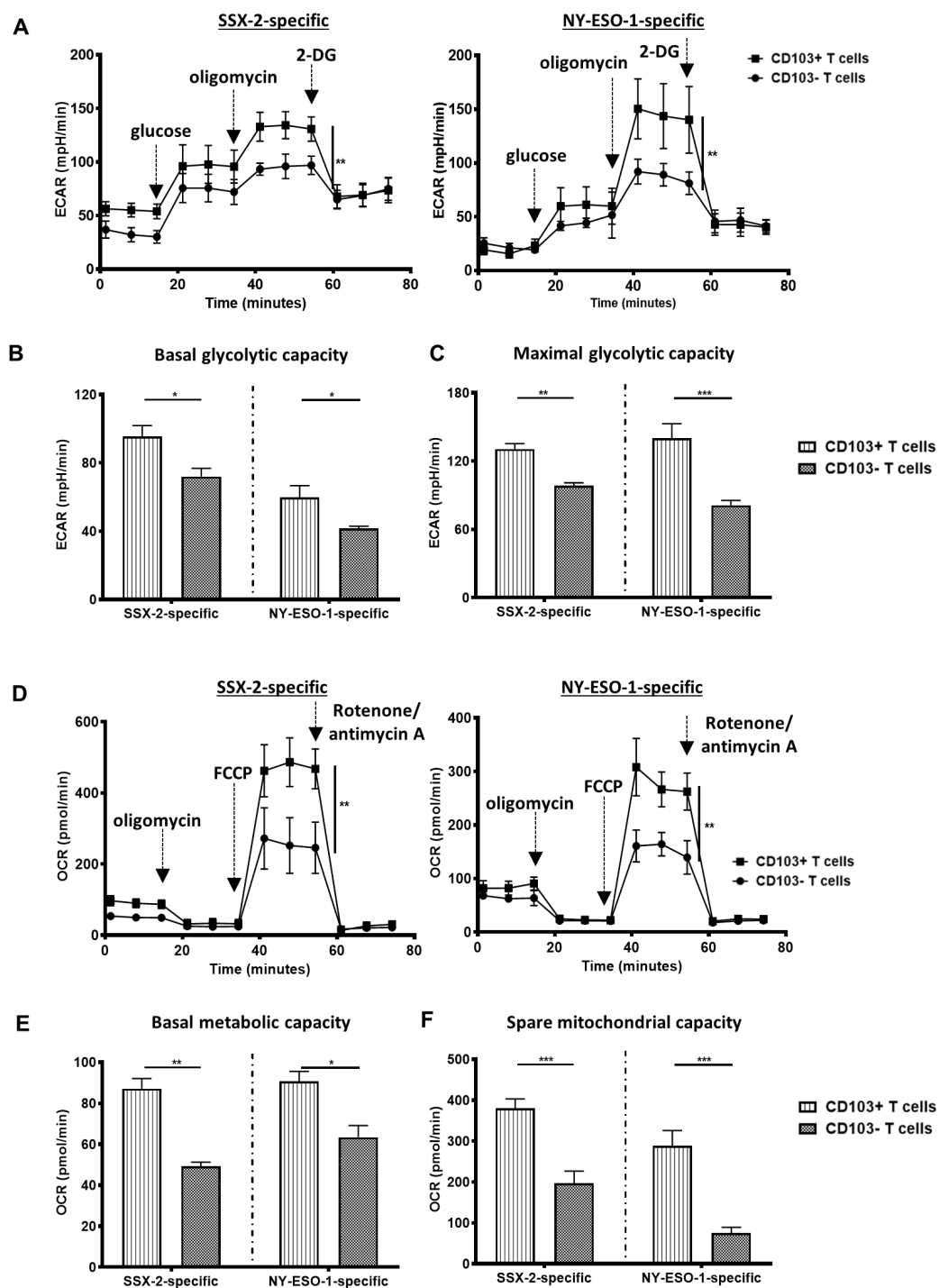


Figure 5

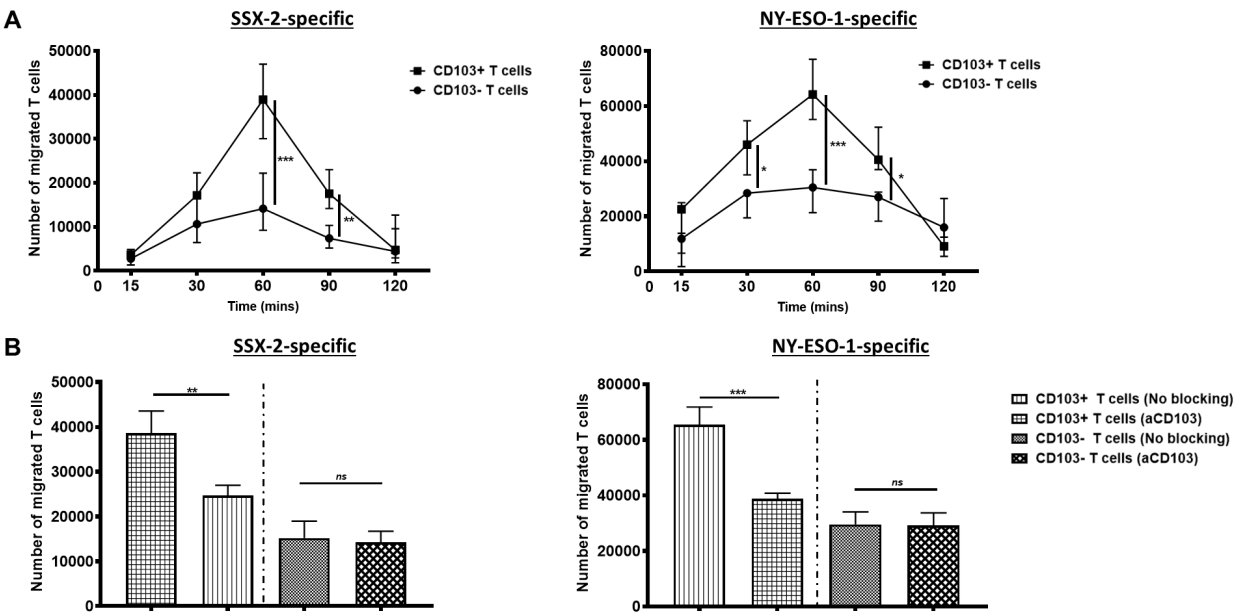


Figure 6

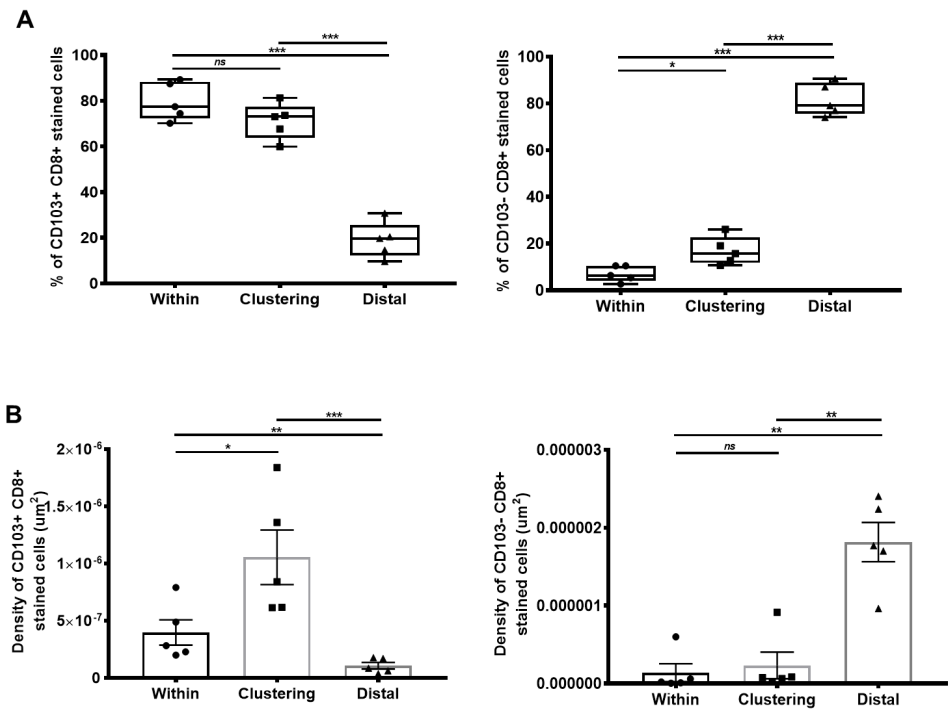


Figure 7

